Title	Intrafractional tracking accuracy in infrared marker-based hybrid dynamic tumour-tracking irradiation with a gimballed linac.
Author(s)	Mukumoto, Nobutaka; Nakamura, Mitsuhiro; Yamada, Masahiro; Takahashi, Kunio; Tanabe, Hiroaki; Yano, Shinsuke; Miyabe, Yuki; Ueki, Nami; Kaneko, Shuji; Matsuo, Yukinori; Mizowaki, Takashi; Sawada, Akira; Kokubo, Masaki; Hiraoka, Masahiro
Citation	Radiotherapy and oncology : journal of the European Society for Therapeutic Radiology and Oncology (2014), 111(2): 301-305
Issue Date	2014-05
URL	http://hdl.handle.net/2433/188903
Right	© 2014 Elsevier Ireland Ltd.
Type	Journal Article
Textversion	author

1   **Intrafractional tracking accuracy in infrared marker-based hybrid**

2   **dynamic tumour-tracking irradiation with a gimballed linac**

3

4   **Nobutaka Mukumoto[a], Mitsuhiro Nakamura[a,*], Masahiro Yamada[a], Kunio**

5   **Takahashi[b], Hiroaki Tanabe[c], Shinsuke Yano[d], Yuki Miyabe[a], Nami Ueki[a], Shuji**

6   **Kaneko[a], Yukinori Matsuo[a], Takashi Mizowaki[a], Akira Sawada[a,e], Masaki Kokubo[c,f],**

7   **and Masahiro Hiraoka[a]**

8   [a] Department of Radiation Oncology and Image-applied Therapy, Graduate School of

9   Medicine, Kyoto University, Kyoto, Japan

10   [b] Advanced Mechanical Systems Department, Mitsubishi Heavy Industries Ltd, Hiroshima,

11   Japan

12   [c] Division of Radiation Oncology, Institute of Biomedical Research and Innovation, Hyogo,

13   Japan

14   [d] Division of Clinical Radiology Service, Kyoto University Hospital, Kyoto, Japan

15   [e] Department of Radiological Technology, Faculty of Medical Science, Kyoto College of

16   Medical Science, Kyoto, Japan

17   [f] Department of Radiation Oncology, Kobe City Medical Center General Hospital, Hyogo,

18   Japan

19

20   *** Corresponding author:** Mitsuhiro Nakamura, Ph.D., Graduate School of Medicine,

21   Kyoto University, 54 Kawahara-cho, Shogoin, Sakyo-ku, Kyoto, 606-8507, Japan.

22   Tel.: +81-75-751-3762; Fax: +81-75-771-9749; E-mail: m_nkmr@kuhp.kyoto-u.ac.jp

23

24   Total number of pages: 16 (**Tables**: 2; **Figures**: 2; **Supplementary Material**: 1)

25

26   **Running title**: Intrafractional accuracy of IR Tracking

27

28   **Key words**: Four-dimensional image-guided radiotherapy, dynamic tumour-tracking

29   irradiation, respiratory motion, Vero4DRT, intra-fractional tracking accuracy.

30

31   **Meeting presentation**: This work was accepted for presentation during the poster viewing

32   session of the 54th Annual Meeting of the American Society for Radiation Oncology in

33   Boston, October 28-31, 2012.

34

35   **ABSTRACT**

36   **Purpose**: To verify the intrafractional tracking accuracy in infrared (IR) marker-based

37   hybrid dynamic tumour tracking irradiation ("IR Tracking") with the Vero4DRT.

38   **Materials and Methods**: The gimballed x-ray head tracks a moving target by predicting its

39   future position from displacements of IR markers in real-time. Ten lung cancer patients

40   who underwent IR Tracking were enrolled. The 95th percentiles of intrafractional

41   mechanical (iE_M^{95}), prediction (iE_P^{95}), and overall targeting errors (iE_T^{95}) were calculated

42   from orthogonal fluoroscopy images acquired during tracking irradiation and from the

43   synchronously acquired log files.

44   **Results**: Averaged intrafractional errors were (left-right, cranio-caudal [CC],

45   anterior-posterior [AP]) = (0.1 mm, 0.4 mm, 0.1 mm) for iE_M^{95}, (1.2 mm, 2.7 mm, 2.1 mm)

46   for iE_P^{95}, and (1.3 mm, 2.4 mm, 1.4 mm) for iE_T^{95}. By correcting systematic prediction

47   errors in the previous field, the iE_P^{95} was reduced significantly, by an average of 0.4 mm

48   in the CC ($p < 0.05$) and by 0.3 mm in the AP ($p < 0.01$) directions.

49   **Conclusions**: Prediction errors were the primary cause of overall targeting errors, whereas

50   mechanical errors were negligible. Furthermore, improvement of the prediction accuracy

51   could be achieved by correcting systematic prediction errors in the previous field.

52

INTRODUCTION

53

54 Respiratory motion is one of the factors causing uncertainties during beam delivery,

55 particularly for thoracic and abdominal tumours [1, 2]. In hypofractionated stereotactic

56 body radiotherapy for lung cancer patients, addition of a large margin to compensate for

57 respiratory motion increases the probability of complications [3]. Several techniques,

58 including forced shallow-breathing, breath-hold, respiratory gating, and dynamic tumour

59 tracking (DTT), have been proposed to reduce the uncertainties caused by respiratory

60 motion [1, 2]. Of these methods, recent interest has focused on the DTT technique, which

61 can reposition the radiation beam dynamically in accordance with the target position. DTT

62 can minimise the internal uncertainties without a burden on the respiration of patients or

63 prolongation of treatment time.

64 We have developed an innovative four-dimensional (4D) image-guided

65 radiotherapy system, the Vero4DRT (MHI-TM2000; Mitsubishi Heavy Industries, Ltd.,

66 Japan, and BrainLAB, Feldkirchen, Germany) [4-10], and used its hybrid DTT irradiation

67 function [infrared (IR)-marker-based hybrid DTT irradiation ("IR Tracking")] clinically in

68 lung cancer patients since September 2011 [10]. In IR Tracking, the position of the target,

69 indicated by implanted fiducial markers, is calculated from external surrogate signals

70 through a pre-built prediction model ("4D model"), and the MV x-ray beam is delivered

71 with real-time monitoring [7, 8, 10-12]. Depuydt et al. showed that the performance of

72 Vero4DRT's DTT function was comparable with other clinical DTT systems in phantom

73 and patient simulation studies [11, 12]. Our group also previously revealed that the

74 accuracy of the 4D model must be verified before treatment, and margins were required to

75   compensate for the prediction error in a phantom study [7]; it was concluded that the

76   accuracy of the 4D model was affected by the baseline drift of respiratory motion [8]. Here,

77   we verified the intrafractional tracking accuracy of IR Tracking for lung cancer patients

78   using intrafractional monitoring images and the corresponding log files.

79

80   **MATERIALS AND METHODS**

81   *The Vero4DRT hybrid dynamic tumour tracking irradiation system*

82   Supplementary Figure 1 (Electronic Appendix) shows a schematic diagram of the

83   Vero4DRT system. The Vero4DRT has several unique components that facilitate DTT

84   irradiation: (1) a compact C-band 6-MV x-ray head with a gimbal mechanism, mounted on

85   an O-ring gantry. The gimballed x-ray head can swing itself in both the pan and tilt

86   directions, (2) gantry-mounted orthogonal kV x-ray imaging subsystems, consisting of two

87   sets of x-ray tubes and flat-panel detectors, with a spatial resolution of 0.2 mm at the

88   isocentre level, and (3) an extended version of the ExacTRAC system that enables real-time

89   motion monitoring and management for the DTT function [7, 8, 11, 12] with an IR camera

90   mounted on the ceiling of the treatment room.

91   Supplementary Figure 2 shows a schematic diagram of the IR Tracking procedure.

92   After patient positioning, a 4D model is created using synchronously monitored internal

93   target motion and an external surrogate signal. The detected target position (P_d) is defined

94   as the tumour centre-of-mass calculated from the positions of the implanted fiducial

95   markers on the x-ray images. The relative shift amount between the tumour centre-of-mass

96   and centroid of the markers' polyhedron was determined at the end-exhalation phase in the

97   planning computed tomography. The predicted target position (P_p) is calculated from the

98   4D model, expressed by a quadratic equation involving two variables, the position and

99   velocity of the IR markers. The positions of the IR markers are predicted linearly from the

100   past motion to compensate for the DTT system delay [11]. Details of the prediction model

101   are described in the Supplementary Materials section. In this 4D-modelling phase, the

102   peak-to-peak amplitude of the detected target motion (A) and the mean (μ) and standard

103   deviation (SD) of the absolute 4D-modelling error (E_{4DM}), defined as the absolute

104   difference between the P_p and P_d, are calculated along each axis automatically. During

105   beam delivery, the future 3D target position is calculated from the displacements of the IR

106   markers using the 4D model, and then the corresponding tracking angle is transferred

107   continuously to the gimballed x-ray head. Additionally, circles with a user-defined radius

108   around the predicted positions of the fiducial markers (tolerance circles) are displayed on

109   the monitoring images as a benchmark in re-modelling. When the fiducial markers are

110   deviated systematically from the tolerance circles, re-modelling should be performed

111   during each treatment session (Fig. 1).

112

113   *Patient characteristics and treatment planning*

114   Ten lung cancer patients who underwent IR Tracking in an Institutional Review

115   Board-approved trial were included in the present study. Patient selection criteria were

116   based on our stereotactic body radiation therapy protocol and written informed consent for

117   the present study was obtained from each patient [3, 10]. Three or more 1.5-mm-diameter

118   gold markers (Olympus Co., Tokyo, Japan) were implanted around the lung tumour

119 transbronchially 1–2 weeks before treatment planning. Table 1 shows the characteristics of

120 the patients and treatment planning. We performed a dry-run treatment session prior to

121 treatment planning to assess the characteristics of respirations and to identify

122 patient-specific planning target volume (PTV) margins [7, 9]. The median of A was 2.8 mm

123 in the left-right (LR), 15.8 mm in the cranio-caudal (CC), and 4.3 mm in the

124 anterior-posterior (AP) directions. The median of $\mu+2SD$ of the E_{4DM} during the dry-run

125 treatment session ($E_{4DM}^{\mu+2SD}$) was 0.6 mm in the LR, 1.9 mm in the CC, and 0.7 mm in the AP

126 directions. Patient-specific PTV margins of 5.0–9.0 mm were added to the tumour along

127 each axis to compensate for intra- and interfractional uncertainties in IR Tracking [7, 9, 13].

128 Supplementary Figure 3 shows the definition of the patient-specific PTV margins. The

129 intra- and interfractional uncertainties were classified into systematic and random

130 components. The patient-specific PTV margins were then calculated for each axis using the

131 formula in Supplementary Figure 3. Prescribed doses of 48 or 56 Gy were specified to

132 isocentre in four fractions. Treatment plans included 6-8 non-coplanar fields, with a dose

133 rate of 500 MU/min.

134

135 ***Data acquisition during beam delivery***

136 During beam delivery, the target and fiducial markers were monitored using orthogonal kV

137 x-ray imaging subsystems at 1 Hz. The predicted target positions and tracking angles of the

138 gimballed x-ray head were recorded in log files at 60 and 200 Hz, respectively. In total,

139 9268 paired images (~30 paired images per field) and corresponding log files were

140 acquired.

141

142 ***Verification of intrafractional tracking accuracy***

143 Intrafractional tracking accuracy was verified by the P_d from the fluoroscopic images and

144 the corresponding P_p and the tracked target position, calculated from the synchronously

145 acquired log files. Supplementary Figure 4 shows the geometric point of the tracked target

146 position at the depth of the P_d ($P_{t,d}$). The tracked target position at the depth of the P_p ($P_{t,p}$),

147 was calculated similarly. Intrafractional mechanical (iE_M), prediction (iE_P), and overall

148 targeting errors (iE_T) were defined as the differences between $P_{t,p}$ and P_p, P_p and P_d, and $P_{t,d}$

149 and P_d, respectively. Details of the calculation process are described in the Supplementary

150 Materials section.

151 The 95$^{\text{th}}$ percentiles of the absolute iE_M (iE_M^{95}), iE_P (iE_P^{95}), and iE_T (iE_T^{95}) during

152 the treatment course were then calculated using the intrafractional monitoring images and

153 the corresponding log files. Pearson correlation coefficients were calculated to assess the

154 relationship between $E_{4DM}^{\mu+2SD}$ during the dry-run treatment session and iE_P^{95} or iE_T^{95}

155 during the treatment course. To further improve the prediction accuracy, the corrected iE_P^{95}

156 was recalculated retrospectively by subtracting the systematic (*i.e.* signed overall mean) iE_P

157 in the previous field excluding the first field after the 4D modelling. A paired *t*-test with a

158 0.05 significance level was performed for statistical analysis.

159

160 **RESULTS**

161 Table 2 summarises iE_M^{95}, iE_P^{95}, iE_T^{95}, and corrected iE_P^{95} for 10 lung cancer patients.

162   Averaged intrafractional tracking errors were (LR, CC, AP) = (0.1 mm, 0.4 mm, 0.1 mm)

163   for iE_M^{95}, (1.2 mm, 2.7 mm, 2.1 mm) for iE_P^{95}, and (1.3 mm, 2.4 mm, 1.4 mm) for iE_T^{95}.

164   Additionally, a strong positive correlation was found between $E_{4DM}^{\mu+2SD}$ and iE_P^{95} (LR, CC,

165   AP) = (0.73 [p = 0.017], 0.82 [p = 0.003], 0.96 [p = 0.000]) or iE_T^{95} (LR, CC, AP) = (0.69

166   [p = 0.028], 0.77 [p = 0.010], 0.90 [p = 0.001]). As shown in Table 2, iE_P^{95} was the

167   primary cause of iE_T^{95}, while iE_M^{95} was negligible. The iE_T^{95} was fully covered by the

168   PTV margin, including the geometric variations between the tumour and fiducial markers.

169   Figure 2 (a) shows representative probability histograms in the positional error in the CC

170   direction for the first patient who underwent IR Tracking (Patient No. 1). iE_T^{95} was

171   2.3 mm for this patient.

172   A maximum iE_T^{95} of 4.1 mm was observed for Patient No. 7 in the CC direction.

173   This patient showed the largest difference between $E_{4DM}^{\mu+2SD}$ and iE_P^{95} [LR, CC, and AP =

174   1.6, 1.5, and 1.6 mm, respectively] due to a baseline drift during beam delivery. Meanwhile,

175   the averaged differences for the other patients were 0.3, 0.6, and 0.7 mm for the LR, CC,

176   and AP directions, respectively. By correcting the systematic prediction errors in the

177   previous field, however, iE_P^{95} decreased, from 4.1 to 2.7 mm, for this patient in the CC

178   direction [Fig. 2 (b)]. The maximum reductions in iE_P^{95} were observed in this patient (LR,

179   CC, AP) = (1.4 mm, 1.4 mm, 0.9 mm). For the entire population, the corrected iE_P^{95} was

180   improved significantly by an average of 0.4 mm in the CC ($p < 0.05$) and by 0.3 mm in the

181   AP ($p < 0.01$) directions.

182

183   **DISCUSSION**

184   The Vero4DRT tracks a moving target in real-time using the orthogonal gimballed x-ray

185   head. In the present study, we established a verification methodology for the intrafractional

186   mechanical, prediction, and overall targeting accuracy in each axis during the treatment

187   course. The 3D coordinates of the intrafractional tracked target position were calculated

188   based on the MV x-ray beam orientation using intrafractional monitoring images and the

189   corresponding log files.

190   We verified the intrafractional tracking accuracy for 10 lung cancer patients who

191   underwent IR Tracking with real-time monitoring. Vero4DRT users can monitor the moving

192   target, fiducial markers, and tolerance circles with its predicted position using orthogonal

193   kV x-ray imaging subsystems during beam delivery. At our institution, the radius of the

194   tolerance circles is set to 3 mm, and the 4D model is re-modelled when the monitored

195   fiducial markers' positions are displaced systematically from the tolerance circles due to

196   baseline drift (Fig. 1). By re-modelling the 4D model, while an iE_T^{95} of less than 3 mm

197   was achieved for nine patients (90%), one patient (Patient No. 7) showed a large iE_T^{95} of

198   greater than 3 mm. The 4D model was updated once during the treatment session for

199   Patient No. 7. However, this patient required additional re-modelling. In IR Tracking, the

200   predominant cause of overall targeting errors was prediction errors. The position and

201   velocity of IR markers involved in the 4D model were predicted linearly from past IR

202   marker motion [8]. Thus, prediction uncertainty of the peak position sometimes

203   overestimated the predicted position of the IR marker and the 4D model enforced a large

204   amplitude of respiration motion (Supplementary Figure 5). In this case, the mechanical

205   response delay of the gimballed x-ray head reduced the impact of the prediction error on

206   the overall targeting error. Thus, the overall targeting errors were sometimes smaller than

207   the prediction errors. Additionally, there were strong correlations between $E_{4DM}^{\mu+2SD}$ and

208   iE_P^{95} or iE_T^{95}, indicating that intrafractional prediction or overall targeting errors during

209   the treatment course could be estimated from 4D modelling errors during the dry-run

210   treatment session. The iE_T^{95} was fully covered by the PTV margin, including a geometric

211   variation between the tumour and fiducial markers of 2.5 mm (Tables 1 and 2). When

212   calculating the PTV margin in IR Tracking, the intra- and interfractional uncertainties

213   should be considered (Supplementary Figure 3). However, the present recipe of the

214   patient-specific PTV margin was tentative so as to perform IR Tracking safely. Therefore,

215   further investigations will be needed to determine the PTV margin size appropriate for IR

216   Tracking [9].

217   The CyberKnife Robotic Radiosurgery System with the integrated Synchrony

218   Respiratory Tracking System (Accuray, Sunnyvale, CA) substantially reduces the

219   geometric error caused by respiratory motion [14, 15]. In the present study, $E_{4DM}^{\mu+2SD}$ was

220   comparable with results of the Synchrony system. However, the correlation between the

221   internal target positions and external surrogates can change in the presence of baseline drift,

222   reducing the accuracy of the prediction model [8, 16]. The Synchrony system periodically

223   updates the prediction model using the intrafractional monitoring images. Updating the 4D

224   model in real-time may also improve the prediction accuracy because the internal/external

225   correlation change or baseline drift in respiration will be corrected. Meanwhile, this is

226   difficult regarding image processing time and minimum interval of the x-ray acquisition

227   during beam delivery. The 4D model in IR Tracking includes the parameters of position and

228   velocity of the IR markers. To update the 4D model, these parameters must be changed.

229   Thus, a shorter monitoring interval would be necessary. In clinical practice, we re-modelled

230   the 4D model at least once during treatment to minimise intrafractional uncertainties due to

231   internal/external correlation change or baseline drift in respiration. However, re-modelling

232   required additional exposures that were 8.3-16.7 times higher than intrafractional

233   monitoring [4, 12]. Also, x-ray image-based DTT, another DTT approach with Vero4DRT

234   [6], would not be an alternative strategy in terms of the difficulty of real-time detection and

235   excessive imaging doses. In the current study, the overall mean errors of iE_P were

236   calculated from around 30 paired images retrieved in the previous field using the

237   monitoring function for the intrafractional tracking accuracy verification. Because the

238   systematic prediction errors resulting from the baseline drift of respiration were reduced by

239   subtracting the overall mean errors of iE_P in the previous field, iE_P^{95} decreased

240   significantly in the CC and AP directions using the monitoring images during beam delivery.

241   In the current study, we used all monitoring images to calculate the systematic prediction

242   errors because iE_P varied according to the respiratory phase. However, a triggered x-ray

243   acquisition based on the respiratory phase would also reduce iE_P^{95} using a small number

244   of monitoring images because the systematic prediction errors could be corrected by the

245   averaged iE_P at the end-expiratory and end-inspiratory phases.

246

247 **CONCLUSIONS**

248 We demonstrated that IR Tracking reduced the impact of respiratory motion substantially.

249 The prediction error was the primary cause of the overall targeting error, while the

250 mechanical error was negligible. The PTV margin fully covered the intrafractional overall

251 targeting errors. The 4D modelling errors during a dry-run treatment session were a good

252 indicator of the prediction and overall targeting errors during the treatment course.

253 Additionally, further improvement in prediction accuracy was achieved by correcting the

254 systematic prediction error in the previous field.

255

256 **CONFLICTS OF INTEREST STATEMENT**

260

261 **ACKNOWLEDGEMENTS**

265

266   **REFERENCES**

267   [1] Keall P J, Mageras G S, Balter J M, *et al*. The management of respiratory motion in

268   radiation oncology report of AAPM task group 76. Med Phys 2006;33:3874–900.

269   [2] Korreman S S. Motion in radiotherapy: photon therapy. Phys Med Biol

270   2012;57:R161–91.

271   [3] Matsuo Y, Shibuya K, Nakamura M, *et al*. Dose-volume metrics associated with

272   radiation pneumonitis after stereotactic body radiation therapy for lung cancer. Int J

273   Radiat Oncol Biol Phys 2012;83:e545–9.

274   [4] Kamino Y, Takayama K, Kokubo M, *et al*. Development of a four-dimensional

275   image-guided radiotherapy system with a gimbaled X-ray head. Int J Radiat Oncol Biol

276   Phys 2006;66:271–8.

277   [5] Takayama K, Mizowaki T, Kokubo M, *et al*. Initial validations for pursuing irradiation

278   using a gimbals tracking system. Radiother Oncol 2009;93:45–9.

279   [6] Mukumoto N, Nakamura M, Sawada A, *et al*. Positional accuracy of novel

280   x-ray-image-based dynamic tumor-tracking irradiation using a gimbaled MV x-ray

281   head of a Vero4DRT (MHI-TM2000). Med Phys 2012;39:6287–96.

282   [7] Mukumoto N, Nakamura M, Sawada A, *et al*. Accuracy verification of infrared

283   marker-based dynamic tumor-tracking irradiation using the gimbaled x-ray head of the

284   Vero4DRT (MHI-TM2000). Med Phys 2013;40:041706-1–9.

285   [8] Akimoto M, Nakamura M, Mukumoto N, *et al*. Predictive uncertainty in infrared

286   marker-based dynamic tumor tracking with Vero4DRT. Med Phys 2013;40:091705

287   -1–8.

288 [9] Nakamura M, Mukumoto N, Ueki N, *et al*. Estimation of a tracking margin in

289   surrogate signal-based dynamic tumor tracking irradiation with Vero4DRT. Int J Radiat

290   Oncol Biol Phys 2012;84:S851–2.

291 [10]Matsuo Y, Sawada A, Ueki N, *et al*. An initial experience of dynamic tumor tracking

292   irradiation with real-time monitoring using Vero4DRT (MHI-TM2000). Radiother

293   Oncol 2012;103:S64.

294 [11]Depuydt T, Verellen D, Haas O, *et al.* Geometric accuracy of a novel gimbals based

295   radiation therapy tumor tracking system. Radiother Oncol 2011;98:365-72.

296 [12]Depuydt T, Poelsa K, Verellen D, *et al*. Initial assessment of tumor tracking with a

297   gimbaled linac system in clinical circumstances: A patient simulation study. Radiother

298   Oncol 2013;106:236–40.

299 [13]Ueki N, Matsuo Y, Nakamura M, *et al*. Intra- and interfractional variations in geometric

300   arrangement between lung tumours and implanted markers. Radiother Oncol 2013, in

301   press.

302 [14]Hoogeman M, Prévost J B, Nuyttens J, *et al*. Clinical accuracy of the respiratory tumor

303   tracking system of the cyberknife: assessment by analysis of log files. Int J Radiat

304   Oncol Biol Phys 2009;74:297–303.

305 [15]Pepin E W, Wu H, Zhang Y, *et al*. Correlation and prediction uncertainties in the

306   cyberknife synchrony respiratory tracking system. Med Phys 2011;38:4036-44.

307 [16]Malinowski K, McAvoy T J, George R, *et al*. Incidence of changes in

308   respiration-induced tumor motion and its relationship with respiratory surrogates

309   during individual treatment fractions. Int J Radiat Oncol Biol Phys 2012;82:1665–73.

310

311   **FIGURE LEGENDS**

312   **Figure 1.** Screen shot of the Vero4DRT during infrared (IR)-marker-based DTT irradiation

313   ("IR Tracking"). Monitored fiducial markers' positions were located outside of the

314   "Tolerance circle" displayed around the predicted fiducial markers' positions due to the

315   baseline drift of respiration.

316

317   **Figure 2.** Probability histograms of positional errors in the cranio-caudal (CC) direction (a)

318   for the first patient who underwent IR Tracking (Patient No. 1) and (b) for the most

319   improved patient with intrafractional prediction error (iE_P) correction (Patient No. 7). The

320   Vero4DRT reduced the motion blurring effect caused by respiration.

TABLES

Table 1. Characteristics of the patients and treatment planning.

Patient no.	Age (y.o.)	Sex	Tumour stage	Tumour side	Tumour location	A [mm]			$E_{4DM}^{\mu+2SD}$ [mm]			GTV [cc]	PTV margin [mm]			PTV [cc]
						LR	CC	AP	LR	CC	AP		LR	CC	AP	
1	85	F	Metastasis	Rt	S6	2.2	14.8	2.2	0.2	1.4	0.6	38.7	5.0	7.0	5.0	87.0
2	82	M	T1a	Rt	S9	4.6	19.8	4.4	1.6	3.3	0.5	11.0	5.0	8.0	5.0	34.6
3	86	F	T1b	Rt	S9	2.2	26.0	5.3	0.2	1.6	0.8	12.4	5.0	8.0	5.0	38.0
4	84	M	T1b	Rt	S6	0.9	11.9	3.1	0.3	1.3	0.7	17.8	5.0	7.0	5.0	50.1
5	71	M	T1b	Rt	S5	7.4	3.4	5.1	1.3	1.0	0.7	12.5	5.0	5.0	5.0	33.6
6	87	M	T1b	Lt	S8	2.9	29.6	15.5	0.6	2.2	3.9	20.6	5.0	8.0	8.0	64.1
7	61	M	T2a	Rt	S10	1.4	8.8	4.0	0.5	2.6	0.7	31.9	5.0	6.5	5.0	74.2
8	85	M	T1a	Lt	S9	5.8	30.6	8.7	2.1	3.4	2.9	8.9	5.0	9.0	6.0	33.4
9	68	M	Metastasis	Lt	S8	2.7	9.9	2.3	0.2	0.9	0.4	2.3	5.0	5.0	5.0	10.4
10	60	M	Metastasis	Rt	S9	3.1	16.7	4.1	0.9	2.2	1.6	13.3	5.0	7.0	5.0	38.9

Abbreviations: A=peak-to-peak amplitude of respiration, $E_{4DM}^{\mu+2SD}$= mean plus two standard deviations of the absolute 4D-modelling error during a dry-run treatment session, GTV=gross tumour volume, PTV=planning target volume, LR=left-right, CC=cranio-caudal, AP=anterior-posterior, F=Female, M=Male, Rt=Right lobe, Lt=Left lobe, S= pulmonary segment.

Table 2. iE_M^{95}, iE_P^{95}, iE_T^{95}, and corrected iE_P^{95}.

Patient no.	iE_M^{95} [mm]			iE_P^{95} [mm]			iE_T^{95} [mm]			Corrected iE_P^{95} [mm]		
	LR	CC	AP	LR	CC	AP	LR	CC	AP	LR	CC	AP
1	0.1	0.3	0.1	0.6	2.7	1.3	0.9	2.3	1.0	0.6	1.9	1.2
2	0.3	0.7	0.2	1.4	3.4	0.8	1.3	3.0	0.7	1.3	3.1	0.6
3	0.1	0.4	0.1	0.7	2.5	1.5	0.8	2.2	1.0	0.7	2.7	1.3
4	0.1	0.4	0.1	0.8	2.0	1.5	0.8	1.7	1.0	0.8	1.7	1.4
5	0.1	0.1	0.1	1.8	1.5	1.6	1.1	1.5	1.2	1.5	1.5	1.6
6	0.1	0.3	0.1	1.0	2.5	5.0	1.9	2.3	2.9	0.9	1.8	4.3
7	0.2	0.8	0.2	2.1	4.1	2.3	1.4	4.1	1.6	0.7	2.7	1.4
8	0.2	0.4	0.1	2.1	3.2	3.4	2.2	2.8	1.6	2.5	3.2	3.2
9	0.1	0.3	0.1	0.5	1.6	1.4	0.8	1.4	0.9	0.4	1.3	1.1
10	0.1	0.3	0.1	1.1	3.0	2.0	1.3	2.9	1.6	1.0	2.7	1.8
Average	0.1	0.4	0.1	1.2	2.7	2.1	1.3	2.4	1.4	1.0	2.3	1.8

Abbreviations: iE_M^{95} =95th percentiles of the absolute intrafractional mechanical error, iE_P^{95} =95th percentiles of the absolute intrafractional prediction error, iE_T^{95} =95th percentiles of the absolute intrafractional overall targeting error, LR=left-right, CC=cranio-caudal, AP=anterior-posterior.

Figure 1

(a)

Positional error in CC direction [mm]

(b)

Positional error in CC direction [mm]
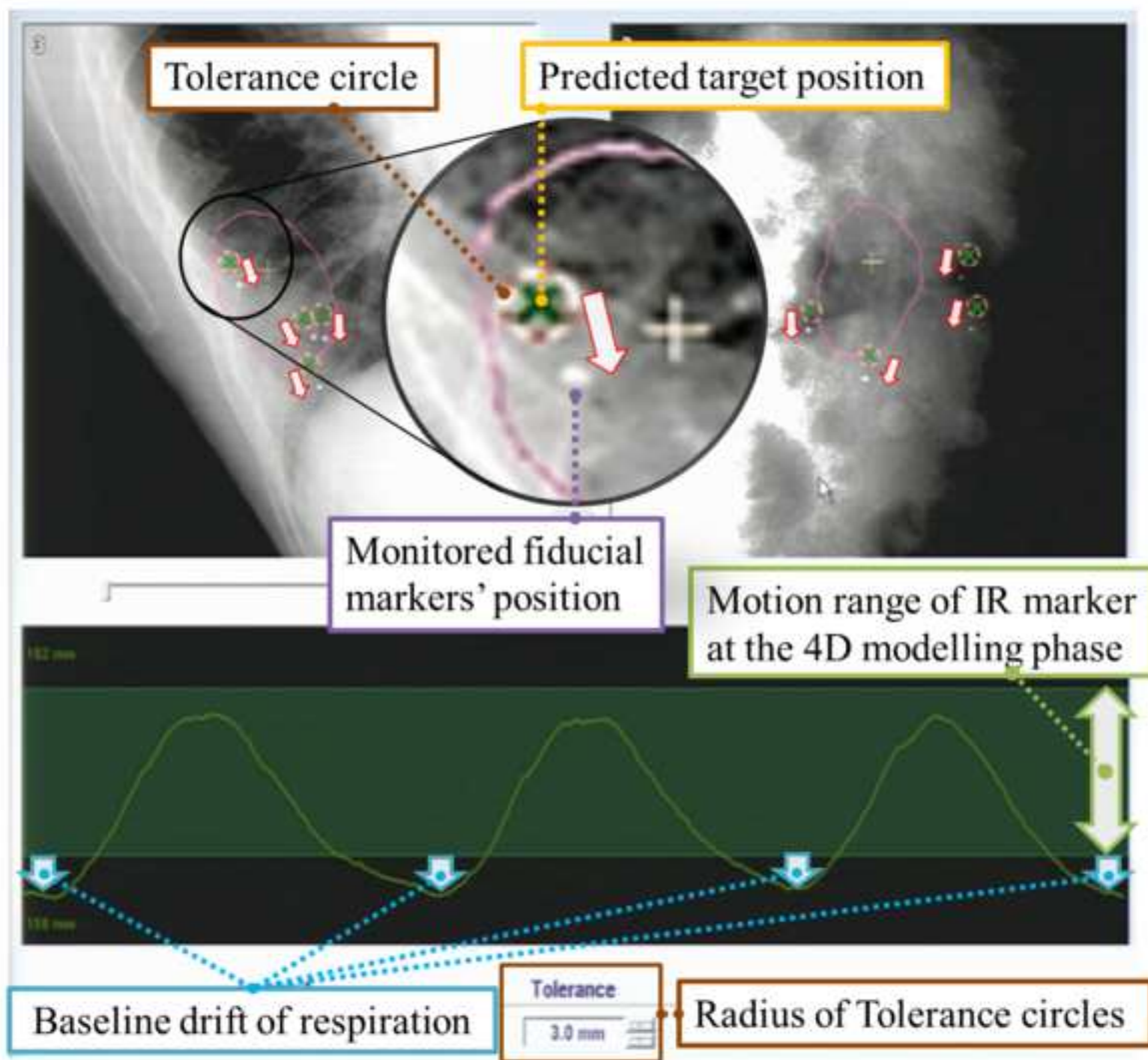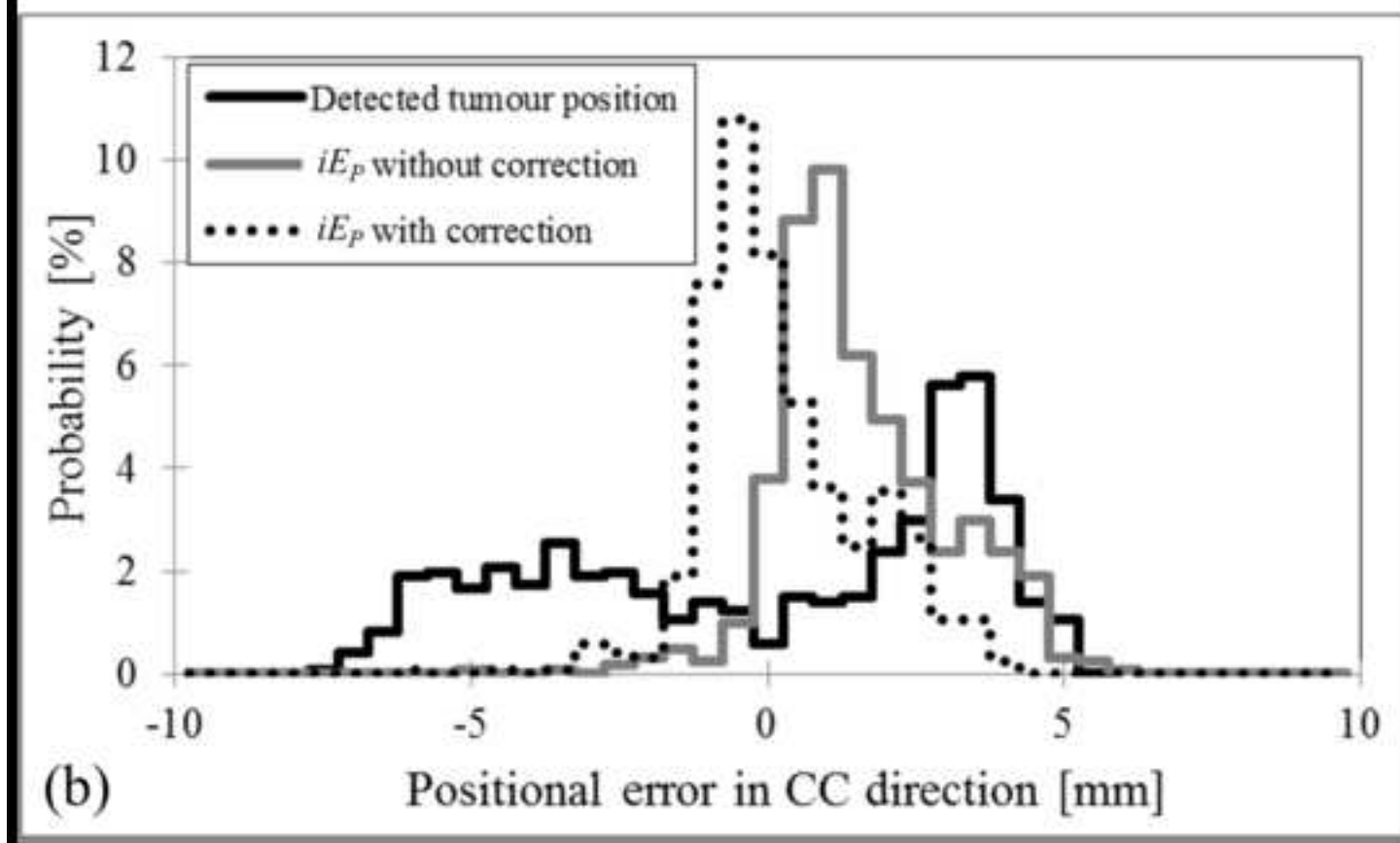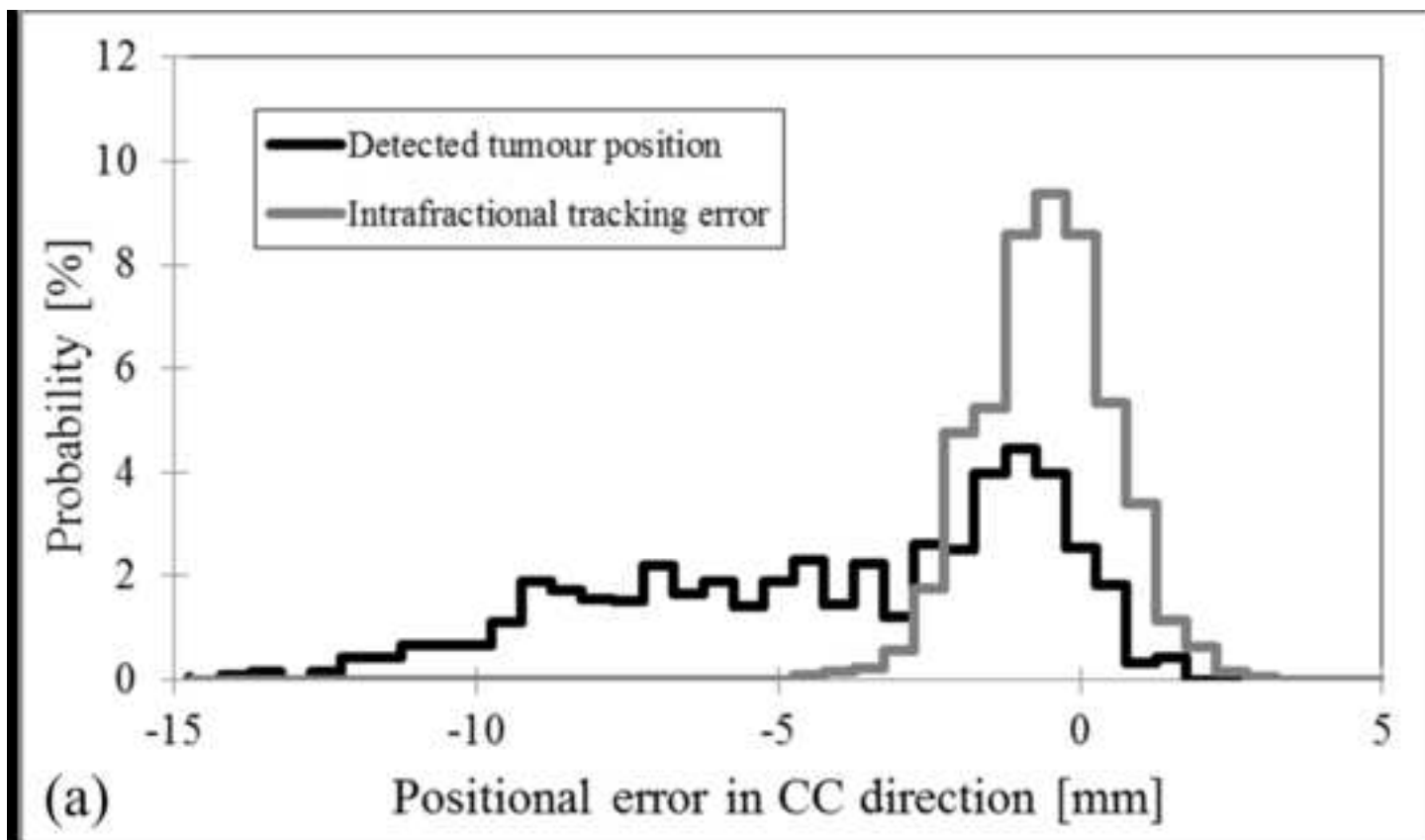
1   ***Prediction model of the Vero4DRT***

2   Before irradiation, a prediction model ("4D model") was created. Infrared (IR) marker

3   displacements and the implanted fiducial markers' motions were monitored for 20-40 s

4   using the IR camera of the ExacTRAC system every 16.7 ms and the orthogonal kV x-ray

5   imaging subsystems every 80 or 160 ms, respectively. The frame rate of x-ray monitoring

6   changed automatically depending on IR marker velocity.

7   After monitoring, two target positions are determined: the detected target position

8   (P_d) and the predicted target position (P_p). The P_d is defined as the tumour centre-of-mass

9   calculated from the positions of the implanted fiducial markers on the x-ray images. The

10   relative shift amount between the tumour centre-of-mass and centroid of the markers'

11   polyhedron was determined at the end-exhalation phase in the planning computed

12   tomography. The positions of the implanted fiducial markers were detected automatically

13   based on the intensity ratios of the fiducial markers to their surroundings with an accuracy

14   of 0.2 mm. The P_p is calculated from the predicted position and velocity of IR markers

15   using the 4D model, expressed as follows:

16
$$P_p = \begin{pmatrix} x_p \\ y_p \\ z_p \end{pmatrix} = \frac{1}{n} \begin{pmatrix} \sum_{i=1}^{n}(a_{x,i}s_i^2 + b_{x,i}s_i + c_{x,i} + d_{x,i}v_i^2 + e_{x,i}v_i) \\ \sum_{i=1}^{n}(a_{y,i}s_i^2 + b_{y,i}s_i + c_{y,i} + d_{y,i}v_i^2 + e_{y,i}v_i) \\ \sum_{i=1}^{n}(a_{z,i}s_i^2 + b_{z,i}s_i + c_{z,i} + d_{z,i}v_i^2 + e_{z,i}v_i) \end{pmatrix} \text{ (equation1)},$$

17   where x_p, y_p, and z_p are the predicted target positions in the left-right, cranio-caudal, and

18   anterior-posterior directions, n is the number of IR markers, and s and v are the predicted

19   position and velocity of each IR marker in the anterior-posterior direction. The positions of

20   the IR markers are predicted from the past motion to compensate for DTT system delay.

21   Parameters of the 4D model (a, b, c, d, and e) were optimised using a least-squares

22   algorithm so that residual errors between the P_p and P_d were minimised.

23   During beam delivery, the future 3D target position is predicted from the

24   displacements of the IR markers using the 4D model, and then the corresponding tracking

25   angle is transferred continuously to the gimballed x-ray head.

26

27   ***Tracked target position calculated from the tracking angle of the gimballed x-ray head***

28   Intrafractional tracking accuracy was assessed by the detected target position (P_d) from the

29   fluoroscopic images and the corresponding predicted target position (P_p) and the tracked

30   target position, calculated from the synchronously acquired log files. The tracked target

31   position was derived from an intersection of a tracking orientation of the gimballed x-ray

32   head with a tracked tumour plane. The tracked tumour plane was defined as the

33   perpendicular plane to the gimbal angle of 0° for each port at the depth of the moving

34   tumour. The tracked target position, based on P_d ($P_{t,d}$), was calculated in the following three

35   steps:

36   (1) Conversion of P_d from room to gantry-ring coordinates:

37
$$\begin{pmatrix} u_d \\ v_d \\ w_d \end{pmatrix} = \begin{pmatrix} \cos G \cos R & -\cos G \sin R & -\sin G \\ -\sin R & -\cos R & 0 \\ \sin G \cos R & -\sin G \sin R & \cos G \end{pmatrix} \cdot \begin{pmatrix} x_d \\ y_d \\ z_d \end{pmatrix} \quad (\text{equation 2}),$$

38   where x_d, y_d, and z_d are the detected target positions along the LR, the CC, and the AP

39   directions in room coordinates, and G and R are the gantry and ring angle, and u_d, v_d, and

40   w_d (units: mm) are the detected target positions in gantry-ring coordinates corresponding to

41   x_d, y_d, and z_d.

42   (2) Calculation of $P_{t,d}$ at the depth of P_d in gantry-ring coordinates

43
$$\begin{pmatrix} u_{t,d} \\ v_{t,d} \\ w_{t,d} \end{pmatrix} = \begin{pmatrix} (960 - w_d) \tan \theta_P \\ (960 - w_d) \tan \theta_T \\ w_d \end{pmatrix} \quad (\text{equation 3}),$$

44   where $u_{t,d}$, $v_{t,d}$, and $w_{t,d}$ (units: mm) are the tracked target positions in gantry-ring

45   coordinates at the depth of the detected target position ($w_{t,d}$). θ_P and θ_T are the pan and

46   tilt angle of the gimballed x-ray head, and 960 mm is the distance from the rotation centre

47   of the gimballed x-ray head to the isocentre.

48   (3) Conversion of $P_{t,d}$ from gantry-ring to room coordinates:

49
$$\begin{pmatrix} x_{t,d} \\ y_{t,d} \\ z_{t,d} \end{pmatrix} = \begin{pmatrix} \cos G \cos R & -\sin R & \sin G \cos R \\ -\cos G \sin R & -\cos R & -\sin G \sin R \\ -\sin G & 0 & \cos G \end{pmatrix} \begin{pmatrix} u_{t,d} \\ v_{t,d} \\ w_{t,d} \end{pmatrix} \quad \text{(equation 4)},$$

50   where $x_{t,d}$, $y_{t,d}$, and $z_{t,d}$ (units: mm) are the tracked target positions in room coordinates. The

51   tracked target position, based on P_p ($P_{t,p}$), at the depth of the predicted target position (w_p)

52   was calculated similarly.

53   Intrafractional mechanical (iE_M), prediction (iE_P), and overall targeting errors (iE_T)
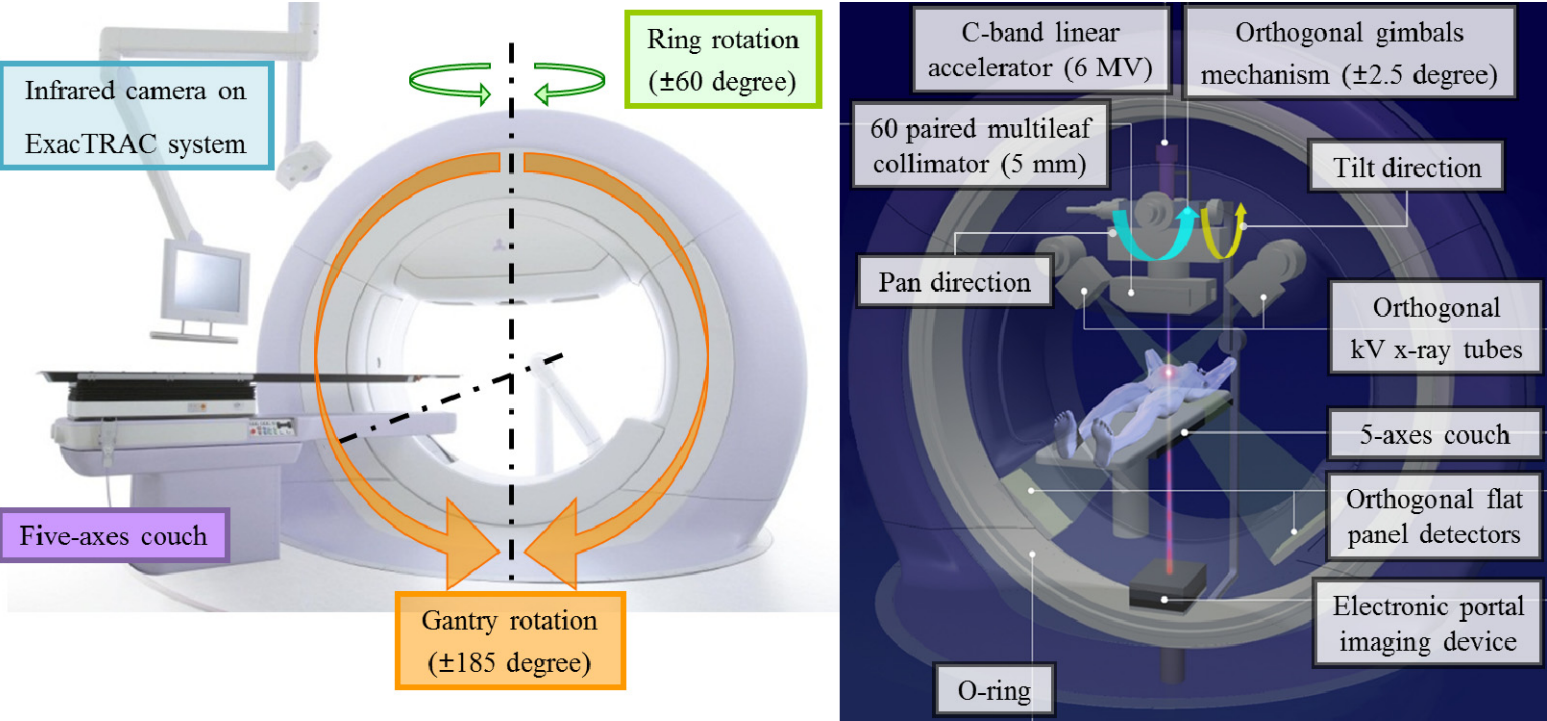
54   were defined as follows:

55
$$iE_M = \begin{vmatrix} x_{t,p} \\ y_{t,p} \\ z_{t,p} \end{vmatrix} - \begin{vmatrix} x_p \\ y_p \\ z_p \end{vmatrix} \quad \text{(equation 5)},$$

56
$$iE_P = \begin{vmatrix} x_p \\ y_p \\ z_p \end{vmatrix} - \begin{vmatrix} x_d \\ y_d \\ z_d \end{vmatrix} \quad \text{(equation 6)},$$

57
$$iE_T = \begin{vmatrix} x_{t,d} \\ y_{t,d} \\ z_{t,d} \end{vmatrix} - \begin{vmatrix} x_d \\ y_d \\ z_d \end{vmatrix} \quad \text{(equation 7)},$$
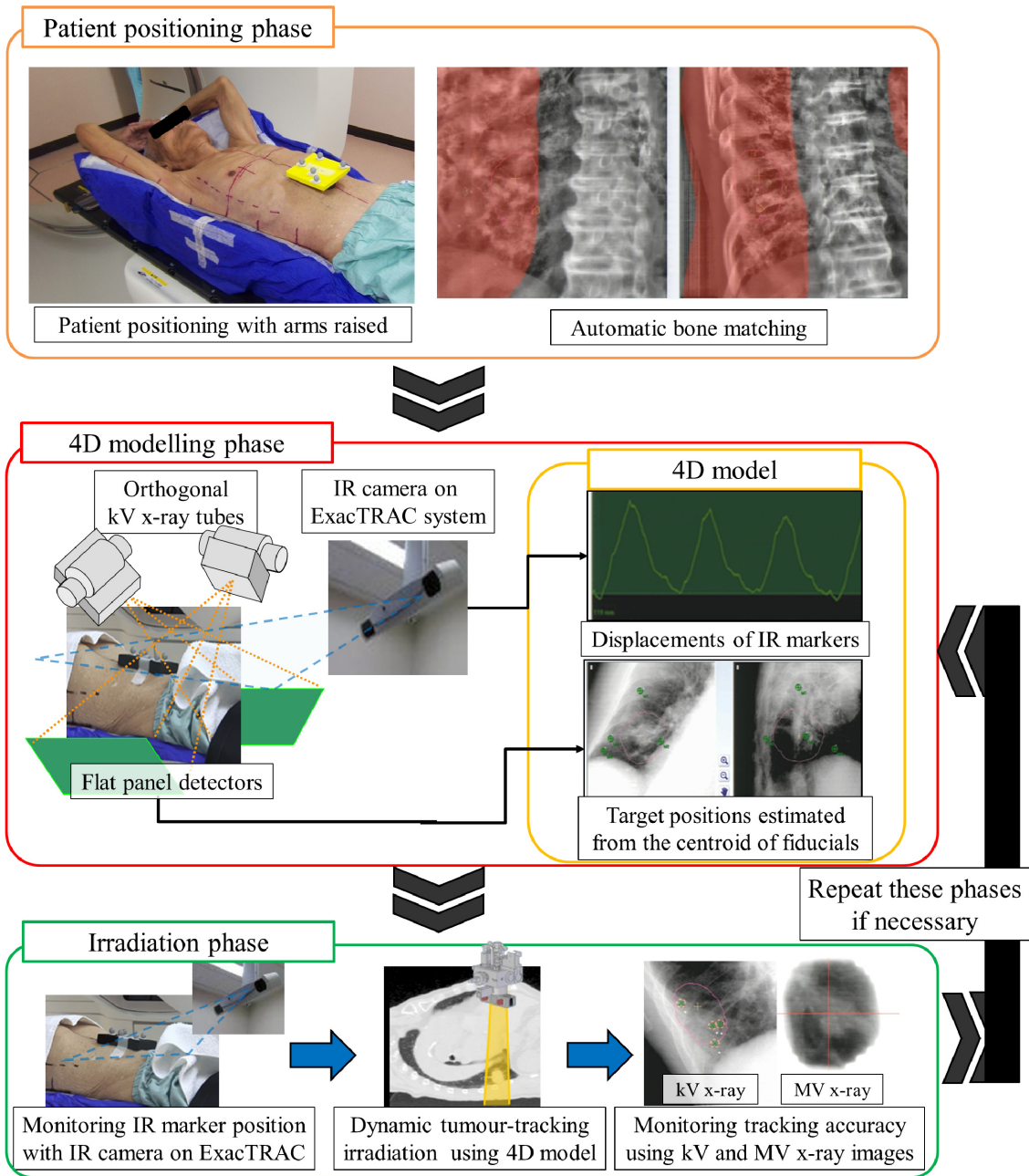
58   where $x_{t,p}$, $y_{t,p}$, and $z_{t,p}$ (units: mm) are the tracked target positions at the depth of the P_p

59   used for the verification of the mechanical error of the gimballed x-ray head against the

60   predicted target positions, and x_p, y_p, and z_p (units: mm) are the predicted target positions

61   used as the tracking commands to the gimballed x-ray head, and x_d, y_d, and z_d (units: mm)

62   are the detected target positions, and $x_{t,d}$, $y_{t,d}$, and $z_{t,d}$ (units: mm) are the tracked target

63   positions at the depth of the P_d used for the verification of the overall targeting error of the

64   gimballed x-ray head against the moving tumour.

65

66 **Supplementary Figure 1**. Schematic diagram of the Vero4DRT system.

Patient positioning phase

Patient positioning with arms raised

Automatic bone matching

4D modelling phase

Orthogonal kV x-ray tubes

IR camera on ExacTRAC system

4D model

Displacements of IR markers

Flat panel detectors

Target positions estimated from the centroid of fiducials

Repeat these phases if necessary

Irradiation phase

Monitoring IR marker position with IR camera on ExacTRAC

Dynamic tumour-tracking irradiation using 4D model

kV x-ray

MV x-ray

Monitoring tracking accuracy using kV and MV x-ray images

67

68 **Supplementary Figure 2**. Infrared (IR) marker-based hybrid dynamic tumour tracking

69 irradiation ("IR Tracking") procedure.

Patient-specific PTV margin

(1) Interfractional error

- Geometric uncertainty between
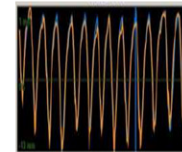 Marker (M_n) and Target (T_n)
  - 2.5 mm
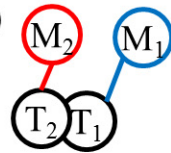
(2) Intrafractional error (Systematic)

- Baseline drift of respiration
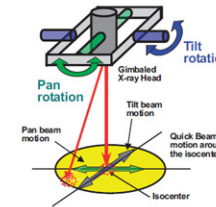 - 10% of peak-to-peak
    Amplitude
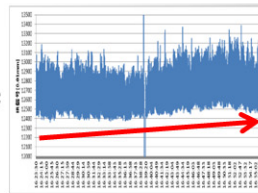
(3) Intrafractional error (Random)

- 4D modelling error
  - Mean + 2SD of absolute
    4D modelling error

(4) Intrafractional error (Random)

- Mechanical error
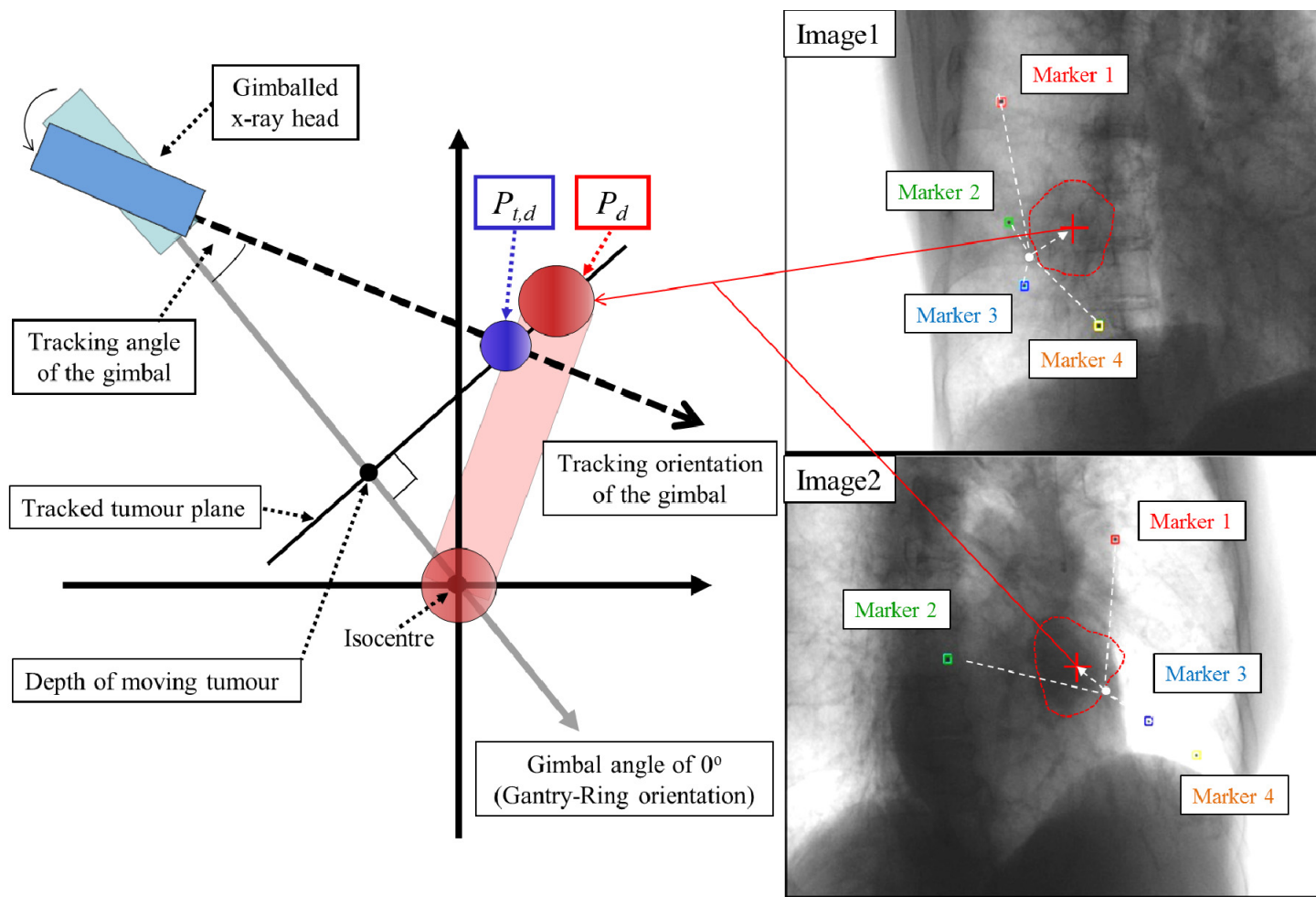 - 95th percentiles
    of mechanical error

$$PTV\ margin\ [mm] = (1) + (2) + \sqrt{(3)^2 + (4)^2}$$
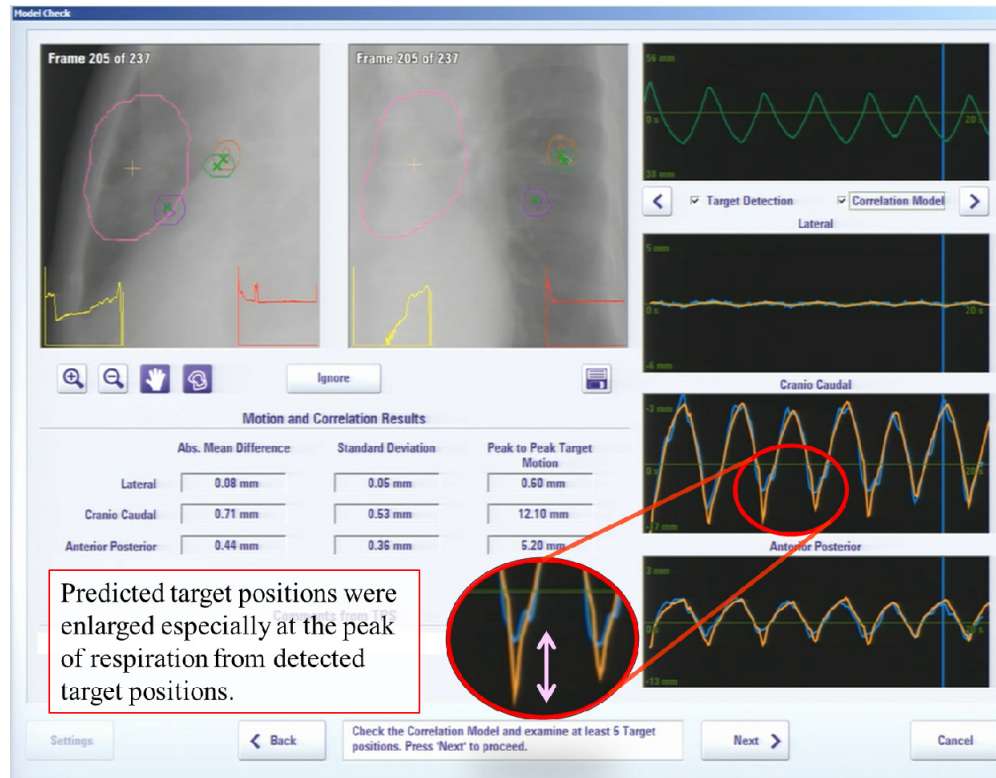$$Minimum\ size\ of\ PTV\ margin\ was\ set\ to\ 5\ mm$$

70

71   **Supplementary Figure 3**. Definition of the patient-specific planning target volume (PTV) margin.

72

Supplementary Figure 4. The geometric point of the tracked target position ($P_{t,d}$) based on the detected target position (P_d)

calculated from orthogonal fluoroscopic images and synchronously acquired log files.

75

Supplementary Figure 5. Screen shot of the Vero4DRT system during creation of the prediction model ("4D model"). The right four groups of waves, from top to bottom, show variations in the infrared (IR) markers' positions in the anterior-posterior direction and the target positions in the lateral, craniocaudal, and anterior-posterior directions, respectively. In the graphs of the target position, dark-coloured waves show the detected target position and light-coloured waves show the predicted target position.